

Interaction and Deformation of Viscoelastic Particles. 2. Adhesive Particles

Phil Attard

Ian Wark Research Institute, University of South Australia, Mawson Lakes SA 5095, Australia

Received January 16, 2001. In Final Form: April 30, 2001

Analyzed is the mutual deformation of adhesive particles that interact with van der Waals forces using a viscoelastic theory that accounts for the time dependence of the phenomenon. The particle shape and interaction is calculated self-consistently for finite-ranged forces. Typical loading–unloading trajectories display hysteresis that increases with driving velocity, as does the particles' adhesion. An analytic approximation that accounts for the precontact deformation is tested against the exact numerical benchmarks and found to be accurate.

Introduction

All solids are elastic, some greatly so, and when they interact they necessarily deform. All solids also experience van der Waals forces, which give rise to attractive interactions and adhesion. The deformation and forces are intrinsically related, and both are large in the region where the surface separation is small. The mutual attraction of solids can be so great as to cause a noticeably flattened contact region whose area is in essence determined by the balance of negative surface energies and positive elastic energies. Such observations have formed the basis for the two widely used theories for particle adhesion, Johnson–Kendall–Roberts (JKR)¹ and Derjaguin–Muller–Toporov (DMT),² which predict that the adhesion should be proportional to the particle radius and surface energy density and that it is independent of the elasticity.

Both JKR and DMT are contact theories that ignore the finite range of the van der Waals interactions. JKR theory in particular ascribes a constant surface energy to the contact region and zero surface energy beyond it. In reality, the contact region has nonzero curvature, which means that the van der Waals energy varies across it, and there is a nonzero interaction between the surfaces beyond the contact region because of the extended range of the van der Waals forces. A further limitation of JKR theory is that it invokes a pressure profile that becomes infinite at the edge of the flattened contact region, whereas on physical grounds the pressure must always remain finite. Derjaguin et al.² avoided the pressure singularity and attempted to take the finite range of the surface force into account by approximating the surface shape as that given by Hertz theory for nonadhesive particles. More sophisticated treatments have treated the deformation and finite-ranged interaction self-consistently by numerically calculating the surface shape and the local pressure, which depends on the local separation.^{3–13} These treatments

suggest that DMT theory is applicable for hard particles with weak interactions and that JKR theory is most relevant for soft, highly adhesive particles.

The difficulty with this simple picture is that as solids become more deformable, they necessarily become more susceptible to viscous and dissipative effects. That is, continuum elasticity theories cannot be applied to very soft materials and instead one has to account for their viscoelastic properties, which among other things means that their deformation becomes time and history dependent. There is overwhelming experimental evidence that the behavior of soft adhesive solids is hysteretic (e.g., see refs 14–21). The facts that the loading and unloading branches do not coincide and that the adhesion depends on the speed of the measurement rules out the application of JKR theory to such materials.

This paper on the viscoelastic problem is motivated by earlier elastic results of the author,⁹ which found for soft solids hysteresis in the force curves and variability in the adhesion. The implication of the result is that JKR theory becomes practically inapplicable in this regime (see the experimental works discussed above). Most recently, Attard^{12,13} has identified the rate dependence of the phenomenon and showed that the adhesion increased with velocity. These calculations were based upon the earlier continuum elasticity theory, which limited the quantitative interpretation of the results.

The present paper is the second in a series for the interaction of viscoelastic particles. The first paper²²

- (1) Johnson, K. L.; Kendall, K.; Roberts, A. D. *Proc. R. Soc. London, Ser. A* **1971**, *324*, 301.
- (2) Derjaguin, B. V.; Muller, V. M.; Toporov, Yu. *J. Colloid Interface Sci.* **1975**, *53*, 314.
- (3) Muller, V. M.; Yushchenko, V. S.; Derjaguin, B. V. *J. Colloid Interface Sci.* **1980**, *77*, 91.
- (4) Muller, V. M.; Yushchenko, V. S.; Derjaguin, B. V. *J. Colloid Interface Sci.* **1983**, *92*, 92.
- (5) Hughes, B. D.; White, L. R. *Q. J. Mech. Appl. Math.* **1979**, *32*, 445.
- (6) Hughes, B. D.; White, L. R. *J. Chem. Soc., Faraday Trans. 1* **1980**, *76*, 963.
- (7) Pethica, J. B.; Sutton, A. P. *J. Vac. Sci. Technol.*, **A** **1988**, *6*, 2490.

- (8) Smith, J. R.; Bozzolo, G.; Banerjee, A.; Ferrante, J. *Phys. Rev. Lett.* **1989**, *63*, 1269.
- (9) Attard, P.; Parker, J. L. *Phys. Rev. A* **1992**, *46*, 7959.
- (10) Parker, J. L.; Attard, P. *J. Phys. Chem.* **1992**, *96*, 10398.
- (11) Greenwood, J. A. *Proc. R. Soc. London, Ser. A* **1997**, *453*, 1277.
- (12) Attard, P. *J. Phys. Chem. B* **2000**, *104*, 10635.
- (13) Attard, P. *Phys. Rev. E* **2001**, *63*, 011601.
- (14) Maugis, D.; Barquins, M. *J. Phys. D: Appl. Phys.* **1978**, *11*, 1989.
- (15) Burnham, N. A.; Dominguez, D. D.; Mowery, R. L.; Colton, R. *J. Phys. Lett.* **1990**, *64*, 1931.
- (16) Chen, Y. L.; Helm, C. A.; Israelachvili, J. N. *J. Phys. Chem.* **1991**, *95*, 10736.
- (17) Chaudhury, M. K.; Owen, M. J. *Langmuir* **1993**, *97*, 5722.
- (18) Creton, C.; Brown, H. R.; Shull, K. *Macromolecules* **1994**, *27*, 3174.
- (19) Deruelle, M.; Leger, L.; Tirrell, M. *Macromolecules* **1995**, *28*, 7419.
- (20) Wahl, K. J.; Stepnowski, S. V.; Unertl, W. N. *Tribol. Lett.* **1998**, *5*, 103.
- (21) Rundolf, M.; Karlsson, M.; Wagberg, L.; Poptoshev, E.; Rutland, M.; Claesson, P. *J. Colloid Interface Sci.* **2000**, *230*, 441.
- (22) Attard, P. *Phys. Rev. E*, in press.

treated nonadhesive particles that interact with electric double layer forces. This paper deals with adhesive particles that interact with van der Waals forces, and it takes into account the nonzero range of their interaction. This distinguishes the present approach from earlier contact theories for adhesive viscoelastic particles. The latter may be divided into two groups: ad hoc formulations that simply modify JKR theory with a somewhat ill-defined time-dependent surface energy^{14,23–25} and theories that are more soundly based on the so-called correspondence principle for viscoelastic deformation.^{26,27} The present paper is likewise based on the latter principle and goes beyond the earlier work in two ways. It avoids the contact approximation by using realistic surface forces, and it treats loading and unloading on an equal footing. (The algorithm can in fact deal with an arbitrary trajectory.²²) In summary, the problem treated here is the deformation and adhesion of two convex viscoelastic particles that interact with van der Waals forces of nonzero range and that are driven together and pulled apart at a uniform velocity.

I. Model and Analysis

A. Viscoelasticity. Viscoelastic materials may be treated by replacing the material parameters of continuum elasticity theory by time-dependent quantities. Using the so-called correspondence principle, the deformation is now given by a time convolution integral in addition to the usual spatial convolution integral over the kernel of continuum elasticity.

For the case of two convex bodies, the separation between their undeformed surfaces at a distance r from the axis is given by $h_0(r) = h_0 + r^2/2R$, where $R = (R_1^{-1} + R_2^{-1})^{-1}$ is the effective radius of the solids. In the case of deformation, the actual local surface separation may be written

$$h(r) = h_0(r) - u(r) \quad (1)$$

The quantity $h_0 \equiv h_0(0)$, which may be positive or negative, is here called the nominal separation, and $h \equiv h(0)$, which must be positive, is called the actual separation. The quantity $u \equiv u(0)$ is called the central deformation (or simply deformation); it is negative when the surfaces are flattened under a positive load, and it is positive when they bulge toward each other or adhere under tension. Invoking the elastic half-space approximation, in continuum linear elasticity theory, the total elastic deformation is given by^{9,31}

$$u(r) = \frac{-2}{\pi E} \int \mathrm{d}\mathbf{s} \frac{p(h(s))}{|\mathbf{r} - \mathbf{s}|} \quad (2)$$

where the elasticity parameter is given in terms of Young's modulus and Poisson's ratio of the bodies, $2/E \equiv (1 - \nu_1^2)/E_1 + (1 - \nu_2^2)/E_2$, and where the kernel is expressible in terms of the complete elliptic integral of the first kind.^{9,31} The integral is over the two-dimensional plane that bisects the bodies, and the element of area is $\mathrm{d}\mathbf{s} = 2\pi s \mathrm{d}s$. Here, $p(h)$ is the pressure between two infinite planes at a separation h ; in the present case, it is taken to have a van der Waals form (see below).

According to the correspondence principle, the generalization of this to viscoelastic materials is^{22,26–29}

$$u(r, t) - u(r, t_0) = \int_{t_0}^t \mathrm{d}t' \frac{-2}{\pi E(t-t')} \int \mathrm{d}\mathbf{s} \frac{\dot{p}(h(s, t'))}{|\mathbf{r} - \mathbf{s}|} \quad (3)$$

where $\dot{p}(h(r, t)) = p'(h(r, t))\dot{h}(r, t)$ is the time rate of change of the pressure. This assumes that the particles are stationary up to time t_0 , $\dot{h}(r, t) = 0$, $t < t_0$, and, if interacting or in contact, have at that time fixed deformation $u(r, t_0) = u_\infty(r, t_0)$, corresponding to static elastic equilibrium. This expression manifests the fact that viscoelastic deformation involves a time integral over the previous history of the material, and it may be verified that this reduces to the static elastic result when $E(t) = \text{const}$.

The effective viscoelastic Young's modulus is time dependent, and its reciprocal is sometimes called the creep compliance function, $C(t) = 1/E(t)$. (Note that the effective viscoelastic modulus $E(t)$ should not be confused with the so-called relaxation function, which is the integral operator inverse of the creep compliance function.²⁷) In general, the instantaneous elastic modulus characterizes the short-time behavior of viscoelastic materials, $C(t) \rightarrow 1/E_0$, $t \rightarrow 0$, and the infinite-time elastic modulus characterizes their long-time behavior, $C(t) \rightarrow 1/E_\infty$, $t \rightarrow \infty$. Viscoelastic materials are initially stiff and soften over time, $E_0 > E_\infty$, which is often called relaxation or creep. The simplest type of viscoelastic material is characterized by the two elastic limits and a characteristic relaxation time τ ,

$$\frac{1}{E(t)} = \frac{1}{E_\infty} + \frac{E_\infty - E_0}{E_0 E_\infty} e^{-t/\tau} \quad (4)$$

Materials of this sort are analyzed in detail here, although it is straightforward to modify the algorithm to deal with materials with multiple relaxation times.²² In principle, the method can also deal with qualitatively different viscoelastic behavior, such as the liquidlike materials studied by Schapery³⁰ and by Hui et al.,²⁶ $C(t) = C_0 + C_1 t^m$, $0 < m < 1$, which corresponds to $E_\infty = 0$.

For the creep compliance functions of the type given in eq 4, it is advantageous to differentiate the deformation equation. This yields²²

$$\dot{u}(r, t) = \frac{-1}{\tau} [u(r, t) - u_\infty(r, t)] - \frac{2}{\pi E_0} \int \mathrm{d}\mathbf{s} \frac{\dot{p}(h(s, t))}{|\mathbf{r} - \mathbf{s}|} \quad (5)$$

Here, u_∞ is the long-time static deformation that would occur if the pressure profile were fixed at its current value,

$$u_\infty(r, t) = \frac{-2}{\pi E_\infty} \int \mathrm{d}\mathbf{s} \frac{p(h(s, t))}{|\mathbf{r} - \mathbf{s}|} \quad (6)$$

As mentioned above, it is assumed that the trajectory starts from the fully relaxed state, $u_\infty(r, t_0) - u(r, t_0) = 0$, which is normally the case if $\dot{p}(t) = 0$, $t < t_0$. The rate of change of the pressure is

$$\dot{p}(h(r, t)) = p'(h(r, t))[\dot{h}_0(t) - \dot{u}(r, t)] \quad (7)$$

where the prime signifies differentiation with respect to argument. Given the current deformation, which fixes $\dot{p}(h(r, t))$, then eq 5 represents a linear integral equation

(23) Falsafi, A.; Deprez, P.; Bates, F. S.; Tirrell, M. *J. Rheol.* **1997**, *41*, 1349.

(24) Barthel, E. *J. Colloid Interface Sci.* **1998**, *200*, 7.

(25) Barthel, E.; Roux, S. *Langmuir* **2000**, *16*, 8134.

(26) Hui, C.-Y.; Baney, J. M.; Kramer, E. J. *Langmuir* **1998**, *14*, 6570.

(27) Lin, Y. Y.; Hui, C.-Y.; Baney, J. M. *J. Phys. D: Appl. Phys.* **1999**, *32*, 2250.

(28) Yang, W. H. *J. Appl. Mech.* **1966**, *33*, 395.

(29) Ting, T. C. T. *J. Appl. Mech.* **1968**, *35*, 248.

(30) Schapery, R. A. *Int. J. Fract.* **1989**, *39*, 163.

(31) Landau, L. D.; Lifshitz, E. M. *Theory of Elasticity*, 2nd English ed.; Pergamon: London, 1970.

for the rate of change of deformation. It can be solved by iteration using the algorithm developed for the static elastic problem.^{9,12} It is then a simple matter of time-stepping to solve the differential equation for a specified trajectory $h_0(t)$, $u(r, t + \Delta t) = u(r, t) + \Delta t \dot{u}(r, t)$.

For the present case of van der Waals forces, the pressure is given by

$$p(h) = \frac{A}{6\pi h^3} \left[\frac{z_0^6}{h_6} - 1 \right] \quad (8)$$

Here, $A \approx 10^{-20}$ J is the Hamaker constant, and $z_0 \approx 0.5$ nm characterizes the short-range soft-wall repulsion; it is the equilibrium separation of planar solids under zero load. This functional form for the van der Waals pressure derives from a Lennard-Jones 6-12 molecular potential. The surface energy is given by $\gamma = A/16\pi z_0^2$, and a dimensionless parameter that characterizes the adhesion is $\sigma = \gamma\sqrt{R/z_0^3} E_\infty^{-2/9}$. The total load is simply the integral of the surface force density,

$$F(t) = 2\pi \int_0^\infty p(h(r, t)) r dr \quad (9)$$

B. Central Deformation Approximation. Attard and Parker⁹ developed an analytic approximation for weak elastic deformations that was shown to give accurate results in the precontact situation. Attard²² developed an analogous approximation for viscoelastic nonadhesive particles that interacted with exponentially decaying double layer forces. The approach is here called the central deformation approximation (CDA), and it consists of replacing the deformation everywhere by its value on the central axis,

$$u(r, t) \approx u(0, t) \equiv u(t) \quad (10)$$

This is accurate near the central axis, which, because of the curvature of the bodies, is the region that dominates the force at large separations. It becomes inaccurate when the deformation varies across the region that contributes to the interaction, which is the case near and beyond contact. Hence, its use is restricted to the large separation, precontact regime.

Defining

$$I_m = \int_1^\infty \frac{dx}{\sqrt{x-1}} x^{-m-1} = \frac{(2m)! \pi}{(2^m m!)^2} \quad (11)$$

and also $c_\alpha = 2A\sqrt{R/2}/3\pi E_\infty$, the CDA of the relaxed deformation, eq 6, is

$$\begin{aligned} u_\infty(t) &= \frac{-4\pi}{\pi E_\infty} \int_0^\infty ds \frac{A}{6\pi} \left[\frac{z_0^6}{h(s, t)^9} - \frac{1}{h(s, t)^3} \right] \\ &= -c_\infty \int_{h(t)}^\infty \frac{dh'}{\sqrt{H-h(t)}} \left[\frac{z_0^6}{(h')^9} - \frac{1}{(h')^3} \right] \\ &= -c_\infty \left[\frac{I_8 z_0^6}{h(t)^{17/2}} - \frac{I_2}{h(t)^{5/2}} \right] \end{aligned} \quad (12)$$

where $h(t) = h_0(t) - u(t)$ is the actual separation. Note that in the first line $ds/|s| = 2\pi ds$ has been used and also that the transformation of the variable of integration in the second line arises from the fact that $h(s, t) = h_0(t) - u(t) + s^2/2R$ is a quadratic function of s . The integral in

the differential equation in (5) becomes in the CDA

$$\begin{aligned} \frac{-2}{\pi E_0} 2\pi \int_0^\infty ds \frac{dp(h(s, t))}{dh(s, t)} \dot{h}(s, t) \\ &= \frac{4}{E_0} \int_0^\infty ds \frac{A \dot{h}(t)}{6\pi} \left[\frac{9z_0^6}{h(s, t)^{10}} - \frac{3}{h(s, t)^4} \right] \\ &= c_0 \dot{h}(t) \int_{h(t)}^\infty \frac{dh'}{\sqrt{H-h(t)}} \left[\frac{9z_0^6}{(h')^{10}} - \frac{3}{(h')^4} \right] \\ &= c_0 (\dot{h}_0(t) - \dot{u}(t)) \left[\frac{9I_9 z_0^6}{h(t)^{19/2}} - \frac{3I_3}{h(t)^{7/2}} \right] \end{aligned} \quad (13)$$

Accordingly, the CDA version of eq 5 for the precontact viscoelastic deformation is

$$\begin{aligned} \dot{u}(t) &= -\tau^{-1} \left(u(t) + c_\infty \left[\frac{I_8 z_0^6}{h(t)^{17/2}} - \frac{I_2}{h(t)^{5/2}} \right] \right) + \\ &\quad c_0 (\dot{h}(t) - \dot{u}(t)) \left[\frac{9I_9 z_0^6}{h(t)^{19/2}} - \frac{3I_3}{h(t)^{7/2}} \right] \\ &= \left\{ \tau c_0 \dot{h}(t) \left[\frac{9I_9 z_0^6}{h(t)^{19/2}} - \frac{3I_3}{h(t)^{7/2}} \right] - u(t) - c_\infty \left[\frac{I_8 z_0^6}{h(t)^{17/2}} - \frac{I_2}{h(t)^{5/2}} \right] \right\} \left\{ \tau + \tau c_0 \left[\frac{9I_9 z_0^6}{h(t)^{19/2}} - \frac{3I_3}{h(t)^{7/2}} \right] \right\} \end{aligned} \quad (14)$$

For a given trajectory $h_0(t)$, the deformation $u(t)$ and hence the actual separation $h(t)$ are readily obtained from this equation for $\dot{u}(t)$ by simple time-stepping.

In the central deformation approximation, the force is given by⁹

$$\begin{aligned} F(t) &= 2\pi \int_0^\infty ds s p(h(s, t)) \\ &= 2\pi R \int_{h(t)}^\infty dh' \frac{A}{6\pi (h')^3} \left[\frac{z_0^6}{(h')^6} - 1 \right] \\ &= 2\pi R \frac{A}{12\pi h(t)^2} \left[\frac{z_0^6}{4h(t)^6} - 1 \right] \end{aligned} \quad (15)$$

This result turns out to be the same as the Derjaguin approximation, except that the planar interaction free energy per unit area is calculated at the actual separation $h(t) = h_0(t) - u(t)$ (as given by the approximation), rather than at the nominal separation $h_0(t)$.

C. Computational Details. The algorithm for solving eq 5 is based upon that used for the elastic problem^{9,12} and has been described previously.²² Briefly, radial functions were stored on a uniform grid of 250–350 points and spacing 6 nm. For particles of radius 10 μm , this gave a separation at the cutoff of more than 100 nm, which is well beyond the range of the surface forces. The drive steps in separation were 0.1–0.01 nm, corresponding to time steps of 10–50 μs . Trajectories were typically started from 10 nm separation, using an equilibrated, fully relaxed surface shape, although in this case the deformation is almost negligible. A triangular drive trajectory was used, with equal and opposite uniform velocities on each branch. The integral equation for the rate of change of deformation, eq 5, was solved by Picard iteration, with automatic adjustment of the mixing parameter up to a value of 10%, depending upon convergence. The iterations were typically

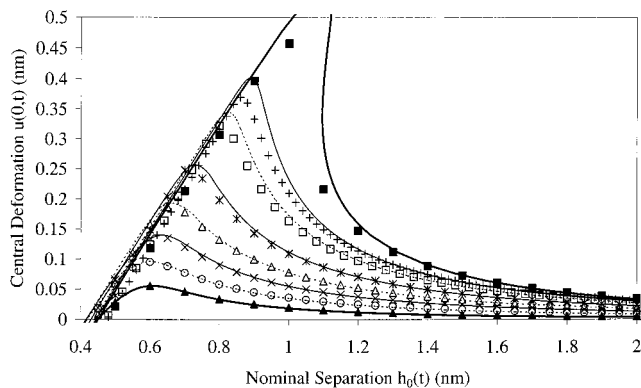


Figure 1. Precontact deformation. The symbols are the full theory, and the curves are the central deformation approximation, eq 14. From top to bottom, the driving velocities are $\dot{h}_0 = -0.1, -0.2, -0.5, -1, -2,$ and $-5 \mu\text{m/s}$. The solid symbols and bold curves are the static results using the infinite time (top, $E_\infty = 10^9 \text{ N m}^{-2}$) and zero time (bottom, $E_0 = 10^{10} \text{ N m}^{-2}$) Young's moduli. The other parameters are $A = 10^{-20} \text{ J}$, $z_0 = 0.5 \text{ nm}$, $\tau = 1 \text{ ms}$, and $R = 10 \mu\text{m}$.

terminated when the change in the central deformation speed was less than 0.1 pm/s , and the change in average deformation speed was less than 0.1 nm/s . At least 20 iterations were used for each time step, and up to several hundred were required in the vicinity of jumps in to and out of contact. The elliptic integrals for the deformation kernel were calculated once using an efficient theta function expansion³² and stored on a quadratic grid, with the logarithmic singularity treated analytically.¹²

Results for purely elastic deformation were also obtained using similar parameters to the above and the previously reported algorithm.^{9,12,22} In the present cases, no hysteresis was found between loading and unloading so one can be certain that these are purely elastic results and that no dissipation or velocity dependence was present.

II. Results

Figure 1 shows the central deformation prior to contact as a function of driving velocity. In general, the deformation is positive, which indicates that the surfaces bulge toward each other under the influence of the van der Waals attraction. By precontact here is meant the region prior to the onset of the short-range repulsion; the nominal separations shown as the abscissa quantify this notion. This effect shows the importance of including the finite range of realistic surface forces, because a contact theory such as JKR or DMT would predict zero deformation in this regime. It may be seen that the viscoelastic deformation at nonzero, finite driving velocities lies between the equilibrium elastic deformation corresponding to the instantaneous and to the long-time elastic moduli. As the velocity slows, the viscoelastic deformation approaches that given by the equilibrium result for the infinite time elastic modulus. Most of the deformation occurs over the distance scale shown in the figure. At the median speed shown, $|\dot{h}_0| = 1 \mu\text{m/s} = 1 \text{ nm/ms}$, it takes approximately twice the relaxation time to cover this distance. Hence, speeds much slower than this yield the long-time equilibrium result, and speeds much faster than this yield the short-time equilibrium result, as indeed the figure shows.

The relatively sudden onset of the soft-wall repulsion causes the bulge to decrease, and it eventually causes the surfaces to flatten ($u(0) < 0$). Here, the particles may be said to be in contact. In this regime, the curves for different

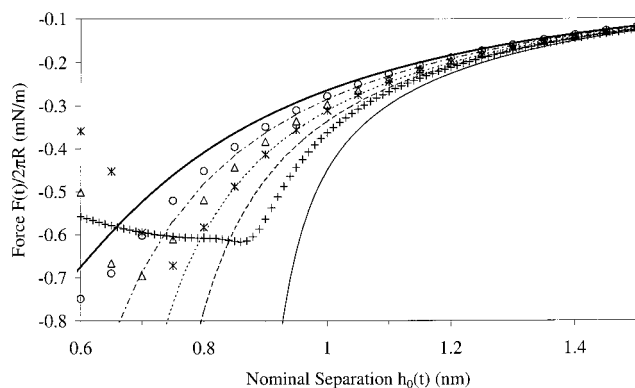


Figure 2. Precontact force. The velocities are, from bottom to top, $\dot{h}_0 = -0.1, -0.5, -1,$ and $-5 \mu\text{m/s}$, respectively. The other parameters are as in the preceding figure. The bold line is the interaction free energy per unit area between rigid planar surfaces.

driving velocities almost coincide. This indicates that in contact the amount of central deformation is, in the main, simply due to geometry rather than to the material parameters of the bodies.

Figure 1 also tests the CDA against the exact results. In all cases shown, it gives very good results for the precontact deformation. At the slower driving speed, it begins to overestimate the bulge near contact, but nevertheless it still correctly estimates the turnover at contact. As an analytic approximation, it is certainly worthwhile.

Figure 2 shows the force just prior to contact. It is attractive because of the domination of the van der Waals tail. The magnitude of the force decreases with increasing driving velocity; the rigid particle case (bold curve) shows the weakest attraction. (This is true approaching contact; the depth of the force minimum actually increases with increasing driving velocity.) These facts indicate that the major effect of elasticity prior to contact is to decrease the actual separation via surface bulging, which results in a stronger force than is indicated by the nominal separation. This interpretation is confirmed by the agreement of the CDA with the exact calculations at larger separations. The only ingredient that goes into the CDA calculation of the force is the approximation for the actual separation. Hence, one may conclude that the change in curvature due to deformation has negligible effect prior to contact. The fact that the CDA begins to overestimate the magnitude of the attraction approaching contact is a manifestation of its overestimate of the bulge just prior to contact. Nevertheless, for these particles one may say that the CDA is a quantitatively accurate approximation beyond about 1 nm separation for these particular particles, with the regime of validity increasing with faster driving speeds.

Figure 3 shows force hysteresis loops for triangular trajectories of the type typically used for loading–unloading experiments. The Hamaker constant that is used here is 10 times larger than in Figure 2, and this is reflected in the order of magnitude deeper minima on approach. This is particularly evident on the magnified scale used in the inset. The fact that the depth of these minima increases with increasing speed and that prior to the minima the magnitude of the attraction decreases with increasing speed is in agreement with the results of Figure 2. On the approach branch in contact, the force increases with decreasing separation. The negative nominal separations and the finite slope of the curve indicate that the particles are flattening under load. The slope

(32) Attard, P.; Mitchell, D. J.; Ninham, B. W. *J. Chem. Phys.* **1988**, *89*, 4358.

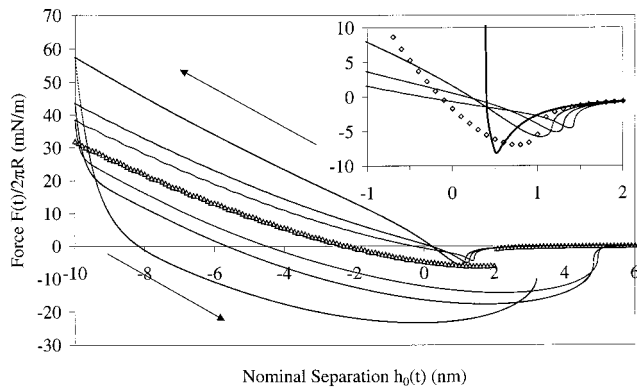


Figure 3. Force in contact. From inside to outside, the hysteresis loops correspond to $|h_0| = 0, 1, 2,$ and $5 \mu\text{m/s}$, with the diamonds being the static result using E_∞ (all parameters as in Figure 1 except that $A = 10^{-19} \text{ J}$). Inset: magnified loading curves. The diamonds are the static result using E_0 , and the bold curve is the force for undeformed particles.

becomes steeper with increasing speed, as one might expect because the stiffness of the viscoelastic particles increases as the time scale decreases.

Following the turning point of the trajectory, the applied load rapidly decreases, with the consequence that the unloading branch lies beneath the loading branch. This gives the hysteresis loop, the size of which increases with increasing driving velocity. The area of the loop corresponds to the energy dissipated in the loading–unloading cycle. Hence, it is a formal requirement that the unloading branch lie below the loading branch; otherwise, one would have the basis for a perpetual motion machine. The general principle is that the force exerted by a system at a given position must be greater than or equal to the force exerted at the same position at a later time, with equality occurring if and only if the system is nondissipative. In Figure 3, the static elastic result corresponding to $E = E_\infty$ is included, and one can see that the hysteresis loops appear to coalesce onto the equilibrium curve as the driving velocity is decreased. Such behavior has been found previously.^{12,13}

The adhesion, which is the force required to separate the particles, (i.e., the maximum tension they can sustain), is given by the minimum force on the unloading branch. In the computations, the separation is controlled, which is the analogue of a fixed grips experiment, and hence the trajectory is able to proceed past the force minimum. A more common experiment controls instead the load or tension, and when the minimum force is attained the system is at a point of unstable equilibrium. It may be seen that the adhesion is significantly greater than the equilibrium prediction and that it increases with increasing driving velocity. Again, this is consistent with recent predictions.^{12,13}

Figure 4 shows the contact radius during the trajectory, with contact signifying surface separations less than 1.1 of the equilibrium separation of planar walls. Although the definition of contact for finite-ranged surface forces is arbitrary, any reasonable definition gives qualitatively similar results to those shown in the figure. As one might expect, the contact area increases on loading and decreases on unloading. For these viscoelastic particles, at a given nominal separation, the contact area is less on loading than on unloading, which reflects the hysteresis in the force curves. The unloading contact radius lags the loading one so that the (nominal) surfaces have to be pulled further apart before they attain the same area as on loading. The unloading branch shows a small but definite increase in the contact area immediately following the turning point.

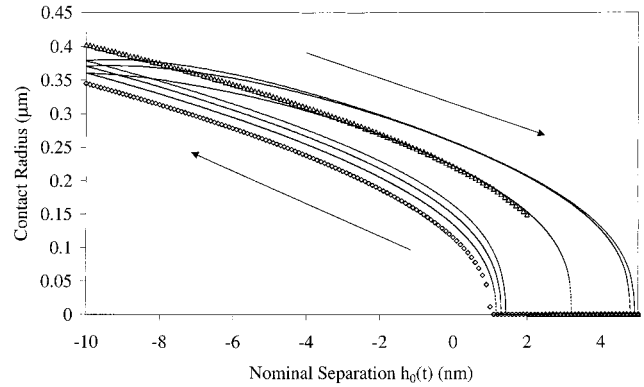


Figure 4. Contact radius. The parameters are as in the preceding figure, with the drive speed increasing from top to bottom on each branch. The triangles are the static result for $E_0 = 10^9 \text{ N m}^{-2}$, and the diamonds are the static result for $E_0 = 10^{10} \text{ N m}^{-2}$. The surfaces were defined to be in contact wherever they were separated by less than $1.1z_0$.

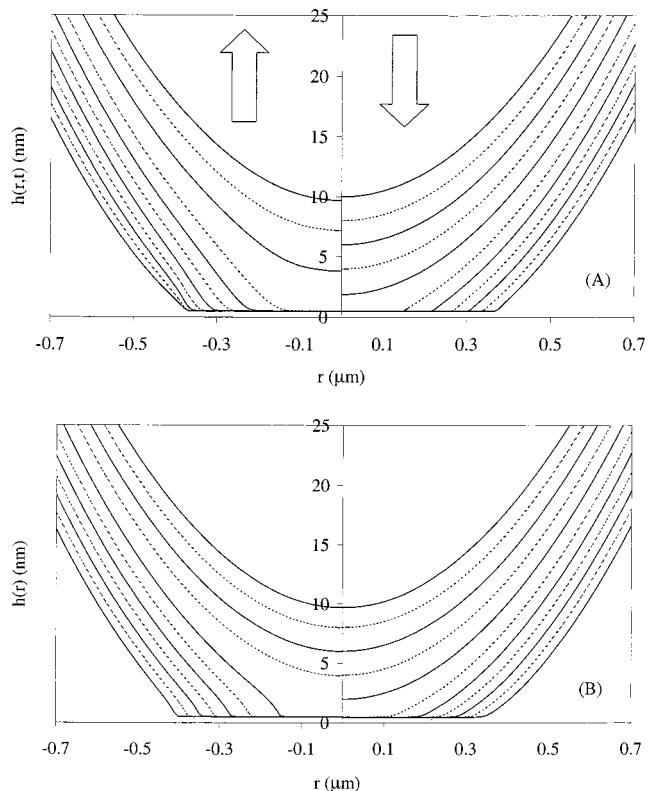


Figure 5. Surface shape. The profiles are plotted every millisecond, or every 2 nm from $h_0 = 10 \text{ nm}$ (top) to -10 nm (bottom). (A) The drive speed is $|h_0| = 2 \mu\text{m/s}$, and $A = 10^{-19} \text{ J}$, with all other parameters as in Figure 1. The right-hand panel is for loading, and the left-hand panel is for unloading. (B) Equilibrium elastic shapes for Young's modulus $E = E_\infty = 10^9 \text{ N m}^{-2}$ (left-hand panel) and for $E = E_0 = 10^{10} \text{ N m}^{-2}$ (right-hand panel).

On each branch, at a given nominal separation, the contact area increases with decreasing drive speed. On the loading branch, it lies between the infinite time and the zero time static elastic results. The adhesion between the particles causes them to spread upon each other, and hence it has a greater effect on soft particles than on hard particles. This rationalizes both the static elastic results and the speed dependence of the viscoelastic results.

Figure 5A shows the shape of the viscoelastic particle during loading and unloading. At the largest separation before loading, the undeformed shape of the spherical

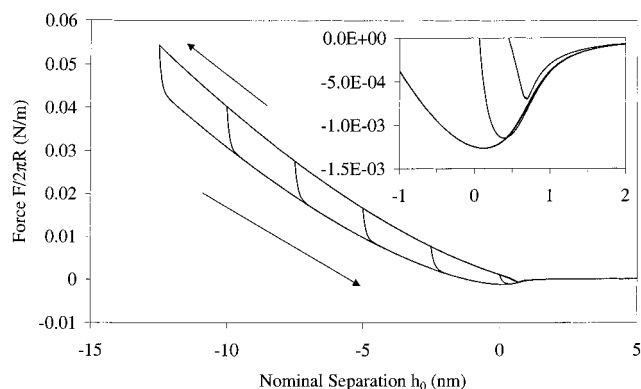


Figure 6. Varying penetrations. The turning point of the trajectory is varied to obtain the force loops corresponding to different penetrations or maximum applied loads. The parameters are as in Figure 1, with $|h_0| = 1 \mu\text{m/s}$. Inset: magnified scale around pull-off.

particle appears parabolic because of the differing scales used on the axes. As the particle is brought toward contact, one can see the slight bulge and elongation of the surface. In contact, there is a relatively well-defined flattened region that grows as the loading is increased. Comparing the two branches in contact, on loading near the contact rim the surfaces appear somewhat rounded, whereas on unloading there is definite extension and stretching evident in the surface shape. This hysteresis in shape has been previously discussed in terms of contact angles, and an analogy has been drawn with solid-on-solid wetting.¹³ Following the relatively rapid jump out of contact, there is a remanent stretching of the surfaces, as may be seen by comparison with the corresponding loading surface profile. This contrasts with the remanent flattening that is observed in the case of nonadhesive particles.²²

It is of interest to compare the shape of the viscoelastic particle with elastic particles that have the long- and short-time elastic moduli (Figure 5B). The shape of the softer particle clearly resembles that of the viscoelastic particle during unloading. It has the same stretched profile and sharper transition at the contact rim and also the sudden jump in to or out of contact. The hard elastic particle has a more rounded shape at the contact rim and a more gradual transition to or from contact on the central axis, both of which feature in the shape of the viscoelastic particle during loading. (Note that these figures show less than 1% of all of the surface profiles actually calculated during an actual trajectory.)

A qualitative comparison of both the viscoelastic and the elastic surface profiles with JKR theory is of interest. As an elastic theory, JKR does not predict any hysteresis or velocity dependence in the surface shape. Furthermore, as a contact theory it is unable to account for the elongation and bulge of the surfaces as they approach each other. Moreover, JKR theory assumes a mathematically flat contact region, whereas in reality that region has finite curvature due to the nonzero range of the surface forces. Finally, JKR theory assumes that the pressure becomes infinite at the edge of the contact zone, whereas in reality it goes smoothly to zero, with the consequence that the surfaces in Figure 5 have a smooth and rounded appearance, which is in contrast to the discontinuity in curvature predicted by JKR theory.

Figure 6 shows the dependence of the force loops on the maximum applied load. After a transient period immediately following the turning point, all the unloading branches meet up and thereafter coincide. It is as if a steady state is reached. This means that the adhesion, or

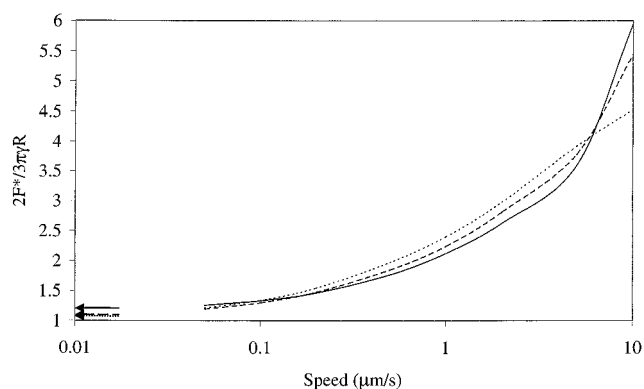


Figure 7. Adhesion. The maximum tension is normalized by the JKR adhesion and shown as a function of the drive velocity (logarithmic scale). The parameters are as in Figure 1, except that $A = 1, 5,$ and $10 \times 10^{-20} \text{ J}$ for the solid, dashed, and dotted curves, respectively. The arrows signify the respective static equilibrium elastic results.

force minimum, will be independent of the maximum applied load. The exception is when the maximum applied load is relatively small (i.e., the time in contact is brief). In these cases, the point at which the trajectory rejoins the envelope of unloading curves is beyond the force minimum of the latter, so that the adhesion is seen to decrease as the maximum applied load decreases. This effect has been seen previously, and Figure 6 is very similar to Figures 5 and 6 of ref 12. This effect should increase with the adhesion parameter σ and with the driving velocity, because both of these increase the size of the hysteresis loop.

Figure 7 shows the pull-off force as a function of the driving velocity. As the velocity is decreased, the curves asymptote to the static equilibrium adhesion. The equilibrium adhesion is greater than that given by the JKR elastic approximation, which is unity on the scale used for the ordinate. The JKR approximation evidently becomes increasingly accurate as the Hamaker constant or surface energy increases and as the time taken for the measurement increases. The system with the smallest Hamaker constant in the figure has surface energy $\gamma = 0.80 \text{ mJ m}^{-2}$ and parameter $\sigma = 0.23$, and that with the largest Hamaker constant has values 10 times greater than these. The results in Figure 7 show that for viscoelastic particles the adhesion increases with increasing speed. This originates in the larger contact area at the time of pull-off because of the increasing lag. For the present parameters, at speeds greater than about $10 \mu\text{m/s}$, there occurs a noticeable dependence of the normalized adhesion on the surface energy, with higher energy particles showing less (normalized) adhesion. The actual adhesion increases with surface energy at all driving velocities. This suggests that at very high speeds the adhesion will be independent of the surface energy.

Summary and Conclusion

In this paper, benchmark results have been obtained for the interaction, adhesion, and deformation of viscoelastic particles that interact with van der Waals forces of nonzero range. Materials with a single relaxation time were modeled, and a range of surface energies and drive velocities were studied. Results were obtained for the precontact deformation and force, the force and area in contact, the deformed surface shape, and the adhesion. The behavior of the particles was found to be hysteretic, with the hysteresis between the loading and the unloading

branches increasing with drive speed. The adhesion or pull-off force was also found to increase with speed.

An analytic approximation was also given, based upon the so-called central deformation approximation developed by Attard and Parker for elastic systems.⁹ The resulting first-order differential equation was readily solved numerically using a spreadsheet, and it was shown to be accurate for the deformation and force in the precontact regime.

It is concluded that the present theory and algorithm represent a tractable and reliable approach to the behavior of interacting adhesive viscoelastic particles. The quantitative analysis of measurements of the adhesion of such

particles should prove feasible and should yield the viscoelastic and surface energy parameters of the materials. Given the success of the central deformation approximation, more refined analytic approximations should also prove worthwhile, particularly in the contact regime.

Acknowledgment. The support of the Australian Research Council through the Special Research Centre for Particle and Material Interfaces at the Ian Wark Research Institute is gratefully acknowledged.

LA010086P